

Parallel quadtree construction on collections of objects

Nathan Morrical, John Edwards*

Idaho State University, Pocatello, ID, USA

Abstract

We present a parallel quadtree algorithm that resolves between geometric objects, modeling space between objects rather than the objects themselves. Our quadtree has the property that no cell intersects more than one labeled object. A popular technique for discretizing space is to impose a uniform grid – an approach that is easily parallelizable but often fails because object separation isn’t known a priori or because the number of cells required to resolve closely spaced objects exceeds available memory. Previous parallel algorithms that are spatially adaptive, i.e., discretizing finely only where needed, either separate points only or make no guarantees of object separation. Our 2D algorithm is the first to construct an object-resolving discretization that is hierarchical (saving memory) yet with a fully parallel approach (saving time). We describe our algorithm, demonstrate experimental results, and discuss extension to 3D. Our results show significant improvement over the current state of the art.

1. Introduction

Constructing quadtrees on objects is an important task with applications in collision detection, distance fields, robot navigation, shape modeling, object description, and other applications. Quadtrees built on objects most often model the objects themselves, providing a space-efficient representation of arbitrarily complex objects. However, our work centers on using quadtrees to separate, or resolve, collections of closely spaced objects, i.e., to construct a discretization such that no cell intersects more than one object. Such quadtrees can be thought of as modeling the space between objects.

Modeling inter-object spacing is computationally straightforward when the spacing is large compared to the world bounding box. Approaches typically involve a uniform grid of the space, which leads to efficient computation that often uses graphics processors.

Difficulties arise when objects are close together relative to the size of the domain. An approach using a uniform grid would have excessive memory requirements in order to resolve between objects because the uniformly sized grid cell must be small enough to fit between objects at every location in the domain. Thus, an adaptive approach must be used for datasets of closely spaced objects.

To our knowledge, only one algorithm [1] computes an adaptive data structure that fully resolves between objects without using unreasonable amounts of memory, but it does so in serial, with expected performance liabilities. A naive approach to parallelizing quadtree computation would be to assign all available compute units according to a coarse grid, then run the serial algorithm on each compute unit. While simple, there is potential for serious load imbalancing if the close object spacings are not uniformly distributed.

This paper extends the work done by Edwards et al. [1] by computing the quadtree in parallel with an algorithm that is adaptive and independent of object distribution. Our algorithm, which is targeted for the GPU, performs an order of magnitude faster than the previous work and will be an important base for later distance transform and generalized Voronoi diagram computation.

Our algorithm has three main components:

1. Construct a quadtree on object vertices using the Karras algorithm [2]
2. Detect quadtree cells that intersect more than one object, which we call “conflict cells” (contribution)
3. Subdivide conflict cells to resolve objects (contribution)

Each step is done in parallel either on object vertices, object facets, or quadtree cells.

*Corresponding author

Email addresses: bitinat2@isu.edu (Nathan Morrical), edwajohn@isu.edu (John Edwards)

53 Modeling object separation is of some use in 2D
54 (e.g. path planning), but it is a very important prob-
55 lem in many 3D applications. Hierarchically subdivid-
56 ing space between faceted objects in a principled paral-
57 lel way is complex, and this paper lays the groundwork
58 for our continuing efforts in 3D.

59 2. Related work

60 **Serial** In an early work, Lavender et al. [3] define and
61 compute octrees over a set of solid models. Two sem-
62 inal works build octrees on objects in order to com-
63 pute the Adaptive Distance Field (ADF) on octree ver-
64 tices. Strain [4] fully resolves the quadtree everywhere
65 on the object surface, and Frisken et al. [5] resolve the
66 quadtree fully only in areas of small local feature size.
67 Both approaches are designed to retain features of a single
68 object rather than resolving between multiple ob-
69 jects, as is required for GVD computation. Boada et
70 al. [6, 7] use an adaptive approach to GVD computa-
71 tion, but their algorithm is restricted to GVDs with con-
72 nected regions and is inefficient for polyhedral objects
73 with many facets. Two other works are adaptive [8, 9]
74 but are computationally expensive and are restricted to
75 convex sites.

76 **Parallel** Many recent works on fast quadtree construc-
77 tion using the GPU are limited either to point sites
78 [10, 2, 11] or to sites that don’t overlap octree cells [12].
79 Most quadtree approaches that support surfaces are de-
80 signed for efficient rendering and not inter-object reso-
81 lution. Most of these approaches construct the quadtree
82 on the CPU [13, 14, 15, 16], although Choi et al. [17]
83 succeed in constructing k-D trees in parallel. Two works
84 [18, 19] implement Adaptive Distance Fields in parallel
85 on quadtrees but building the quadtree itself is done se-
86 quentially. Yin et al. [20] compute the octree entirely on
87 the GPU using a bottom-up approach by initially subdivid-
88 ing into a complete octree, resulting in memory usage
89 that is no better than using a uniform grid. Crassin
90 and Green [21] build the octree top-down by perform-
91 ing subdivisions at each level. The most similar work to
92 what we do here is Kim and Liu’s method [22], which
93 computes the quadtree on the barycenters of triangles,
94 giving an approximation of our quadtree, but without
95 fully resolving between objects. We are unaware of any
96 GPU quadtree construction methods that are fully adap-
97 tive and resolve between objects.

98 3. Algorithm

99 We refer to quadtree leaf cells that intersect two or
100 more objects as “conflict cells.” A necessary and suf-

101 ficient condition for a quadtree to resolve objects is to
102 have no conflict cells. Our approach to computing such
103 a quadtree is in two stages. We first build an initial
104 quadtree, called the “vertex quadtree,” using a set S of
105 point samples. We initialize S to be the object vertices.
106 The second stage is to detect conflict cells in parallel,
107 followed by augmenting S with sample points such that
108 a subsequent quadtree built on S resolves conflict cells.
109 If S changed, then we iterate (see section 3.4.4) which
110 is necessary only if a conflict cell has multiple intersect-
111 ing objects. The number of iterations is minimized by
112 starting from an initial vertex quadtree. This two-stage
113 approach enables us to resolve between objects fully in
114 parallel regardless of object spacing, i.e., we do not it-
115 erate through levels of the quadtree, subdividing as we
116 go.

117 Each step of our algorithm, with the exception of re-
118 solving conflict cells, is independent of dimension and
119 can be used for 3D octree applications. But since point
120 sampling for conflict cell resolution is 2D we will use
121 the term quadtree through the algorithm description
122 for consistency. Our algorithm assumes the objects are
123 faceted where the facets are simplices.

124 3.1. Build initial quadtree

125 Our first step is to build a quadtree on the given set
126 of vertices. We use the Karras algorithm [2] which be-
127 gins by placing the given vertices on a Z-Order curve by
128 computing each vertex’s cooresponding Morton code in
129 parallel. Next, Karras sorts the converted points by us-
130 ing a parallel radix sorter, which has a linear execution
131 time. Our implementation uses the efficient four-way
132 parallel radix sorter described by Ha et al. [23]. Once
133 the Morton codes are sorted, the Z-Order curve can be
134 exploited to construct a binary radix tree in a paral-
135 lel bottom up manner by identifying longest common
136 Morton code prefixes between neighboring points. This
137 resultant binary radix tree can be analyzed in parallel
138 to identify the size and structure of the required vertex
139 quadtree. The strength of this approach lies in the fact
140 that overall performance scales linearly with the number
141 of cores, regardless of the distribution of points. That
142 is, even if a large number of vertices are clustered in a
143 small area, requiring deep quadtree subdivision, only a
144 constant number of parallel calls need be made.

145 3.2. Pruning the quadtree

146 During Karras’ initial binary radix tree (BRT) con-
147 struction, we can prune the BRT to simplify the resultant
148 quadtree. This in turn simplifies the work complexity of
149 conflict cell detection and reduces our overall memory

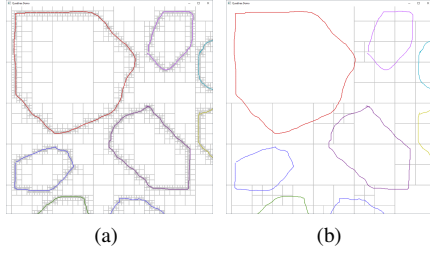


Figure 1: (a) The initial quadtree built on the object vertices, in which no quadtree cell contains more than one vertex, can be far more complex than needed to resolve between objects. (b) After pruning the quadtree. Quadtree cells can contain multiple vertices as long as they all have the same label.

150 footprint. Assume we have a numeric vertex labeling
 151 such that each vertex is labeled to match the object it
 152 belongs to. The original BRT provided by Karras’ al-
 153 gorithm is used to generate a quadtree which separates
 154 vertices regardless of their label. Since our objective is
 155 to resolve between objects of different labels, we can
 156 proactively prune Karras’ initial BRT, and subsequently
 157 the initial quadtree (see figure 1) by allowing the gener-
 158 ated quadtree leaves to contain multiple vertices as long
 159 as those vertices have the same label.

160 To prune the initial BRT efficiently, we label each
 161 BRT node C using the following criterion: if C is a leaf
 162 node that separates two vertices with identical labels, la-
 163 bel C to match the label of the vertices being separated.
 164 If C is a leaf node that separates two vertices having
 165 mismatched colors, label C as “required”. Lastly, if C
 166 is an internal node, i.e., it has children, mark it as “un-
 167 known”. This initial step can be done immediately after
 168 the Karras BRT construction without the need to invoke
 169 an additional kernel.

170 We then propagate the BRT labels up the tree in par-
 171 allel, marking “unknown” nodes as “required” when the
 172 labels of the current node’s two child nodes don’t match.
 173 Labels are applied using an atomic compare and swap,
 174 and threads terminate if the current ancestor’s label was
 175 previously “unknown”. Finally, we generate quadtree
 176 nodes from only the required internal binary radix tree
 177 nodes.

178 3.3. Identifying conflict cells

179 After the pruning in 3.2, the Karras quadtree sepa-
 180 rates all differently labeled vertices in the dataset. Our
 181 goal is to separate differently labeled facets. We first
 182 need to identify what quadtree cells require further sub-
 183 division. We call these cells “conflict cells” (see figure
 184 2c). To efficiently identify conflict cells, we take advan-
 185 tage of the space filling Morton curve and the existing

186 quadtree hierarchy to reduce the combinatoric complex-
 187 ity of intersection detection between facets and quadtree
 188 cells. We use the following approach.

189 3.3.1. Initializing conflict cell detection

190 Before we detect conflict cells we create a mapping
 191 from each quadtree cell c to all facets bounded by c ,
 192 a technique similar in spirit to the fragment emission
 193 and sorting done by Pantaleoni [24]. We first find the
 194 “bounding cell” c_f for a facet f , where the bounding
 195 cell is the smallest quadtree cell that completely con-
 196 tains f . For each facet f in parallel we determine lcp_f ,
 197 which is the longest common prefix of the Morton codes
 198 of the vertices of f . Then, to find the bounding cell c_f ,
 199 we iterate in parallel over each facet f and use lcp_f
 200 to direct a search through the quadtree. Let F be the num-
 201 ber of facets. We allocate two parallel arrays of size F ,
 202 `BCells` and `FacetMap`. As each c_f is found, the index
 203 of c_f is stored in the `BCells` array at index equal to the
 204 thread id. At the same time, we store the index of each
 205 facet in the `FacetMap`. Initially, `FacetMap[i] = i` (see
 206 figure 3a).

207 Next, we perform a parallel radix sort on the paral-
 208 lel arrays (`BCells` and `FacetMap`) using the bounding
 209 cell addresses as the sort key (figure 3b). Finally, since
 210 each quadtree cell may bound multiple facets, we com-
 211 pute a range for each quadtree cell by comparing neigh-
 212 boring quadtree indices in the mapping in parallel (the
 213 `(F/L)Facet` array in figure 3b). We now have a map-
 214 ping from a quadtree cell c to facets bounded by c (fig-
 215 ure 3c).

216 3.3.2. Conflict Cell Detection

217 To identify conflicts, we begin by processing each
 218 leaf cell L in parallel using Algorithm 1. First, we set
 219 L ’s color to -1, meaning it is unknown whether L is a
 220 conflict cell or not. Then, we traverse each direct ances-
 221 tor A of L using a `Parent` field stored in the quadtree data
 222 structure (line 3). For each ancestor traversed, we iter-
 223 ate over the facets bounded by A by using the quadtree
 224 cell to facet mapping computed in 3.3.1 (line 4).

225 For each facet f discovered this way, we test for inter-
 226 section between f and L . If f intersects L and L ’s color
 227 is -1, we copy f ’s color to L . Otherwise if f intersects L
 228 and L ’s color does not match f ’s color, we set L ’s color
 229 to -2, indicating that L is a conflict cell that must be re-
 230 solved. Note that in Algorithm 1, no atomic operations
 231 are required.

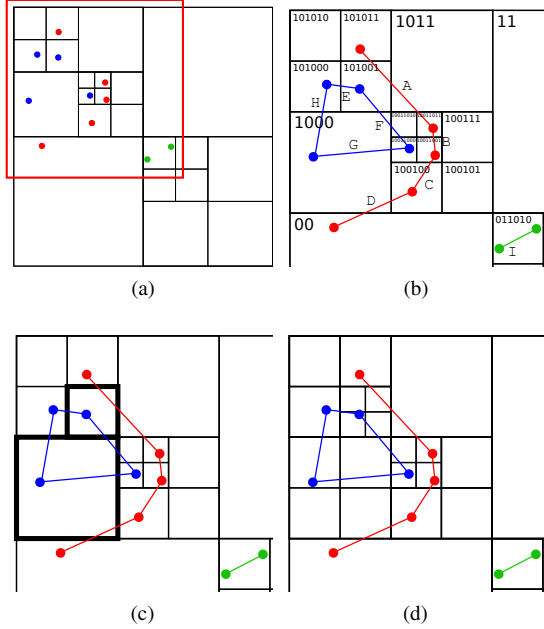


Figure 2: We have three objects, blue, red, and green with facets labeled A-I. (a) Initial pruned vertex quadtree. (b) Zoomed-in to the region outlined by red in (a) and showing the boundary cell (BCell) computation for each facet. (c) Conflict cells, which intersect more than one object, are highlighted. (d) The new quadtree after conflict resolution.

Algorithm 1: FIND_CONFLICT_CELLS

Input: Quadtree

```

1 for leaf cell  $L$  do in parallel
2    $L.color = -1$ 
3   foreach cell  $A$  in  $direct\_ancestors(L)$  do
4     foreach  $i$  in  $\{FFacet[A] \dots LFacet[A]\}$  do
5        $f := Facets[FacetMap[i]]$ 
6       if  $f$  intersects  $L$  then
7         if  $L.color == -1$  then
8            $L.color = f.color$ 
9            $L.facet[0] = f$ 
10        end
11       else if  $L.color \neq f.color$  then
12          $L.color = -2$ 
13          $L.facet[1] = f$ 
14       end
15     end
16   end
17 end
18 end

```

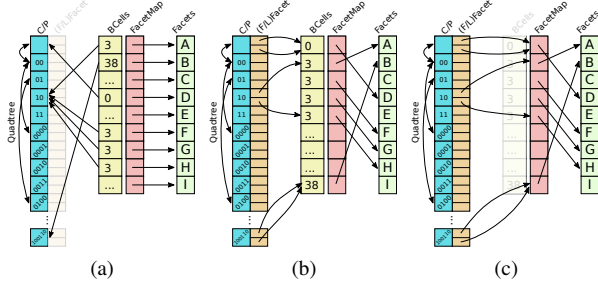


Figure 3: (a) The bounding cells (BCells) are stored in an array initially sorted on facet index (letters are used here for clarity). The quadtree array elements are structures which store child and parent pointers (“C/P” in the figure). (b) We sort the BCells array using a parallel radix sort on BCell address for fast indexed access. We then, in parallel on each element of the BCells array, store the BCells/FacetMap indices of the first and last facets in a given quadtree cell in $FFacet$ and $LFacet$, respectively. (c) For a given quadtree cell, we can find all contained facets for use in algorithm 1.

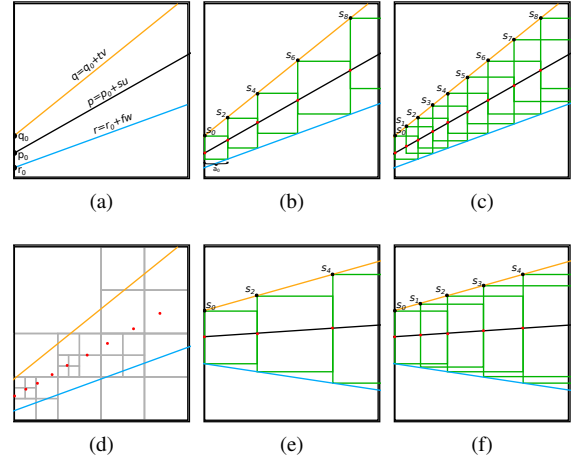


Figure 4: (a) A conflict cell with two lines from different objects. (b)-(c) Fitting boxes such that any box intersecting both lines contains at least one sample (red dots). (b) Fitting boxes such that any box intersecting both lines contains at least two samples. This ensures that a quadtree built from the samples using Karras’ algorithm (panel (d)) will have no leaf cells that intersect both lines, ensuring that the new quadtree is locally free of conflict cells. (e)-(f) The adjacent case.

232 3.4. Resolve conflict cells

233 We present a conflict cell resolution algorithm for
 234 pairs of lines in 2D. For a conflict cell C , our approach
 235 is to find sample points inside the cell such that no leaf
 236 cells in a quadtree constructed over the sample points
 237 intersect both lines. In this section we derive equation
 238 (28) which computes the number of samples required
 239 to resolve the cell. We also derive equation (22) which
 240 computes the samples themselves. The power of our ap-
 241 proach lies in the fact that both expressions are closed-
 242 form and neither one is iterative, so we can evaluate the
 243 first in parallel over leaf cells and the second in parallel
 244 over all samples that we need to compute.

245 To resolve a conflict cell C , we consider pairs of lines
 246 of differing labels that intersect C . Figure 4a shows two
 247 lines

$$q(t) = q = q_0 + tv \quad (1)$$

$$r(f) = r = r_0 + fw \quad (2)$$

along with a line

$$p(s) = p = p_0 + su \quad (3)$$

248 that bisects q and r . Our strategy will be to sample
 249 points P on $p(s)$ (figure 4d) such that a quadtree built
 250 on $S \cup P$ will completely “separate” q and r , i.e., no de-
 251 scendent leaf of C will intersect both q and r . We do this
 252 by ensuring that P is sampled such that every box that
 253 intersects both q and r also intersects at least two points
 254 in P . Because Karras’ algorithm guarantees that every
 255 leaf cell intersects at most one point, we know that no
 256 leaf cell will intersect q and r and thus no leaf cell will
 257 be a conflict cell. We will find a series of boxes such that
 258 each box’s left-most intersection with $p(s)$ is a sample
 259 point meeting the above criterion. In the following discus-
 260 sion, p^x and p^y refer to the x and y coordinates of
 261 point p , respectively.

262 We consider only cases where the slope of p is in the
 263 range $0 \leq m \leq 1$. All other instances can be trans-
 264 formed to this case using rotation and reflection. We
 265 begin by fitting the smallest box centered on a point p
 266 that intersects both q and r . The smallest box sampled
 267 at point $p(s)$ has edge length $a(s)$ as shown in figure 4b.
 268 We break the problem of finding $a(s)$ into two cases:

- 269 1. The *opposite* case (figure 4b) is where $w^y > 0$,
 270 so each box intersects q and r at its top-left and
 271 bottom-right corners, respectively.
- 272 2. In the *adjacent* case (figure 4e), $w^y < 0$, so the
 273 line intersections are adjacent at the top-left and
 274 bottom-left corners of the box.

275 3.4.1. Finding $a(s)$ – opposite case

276 Given a point $p(s)$, we wish to find $a = a(s)$, which
 277 will give us the starting x coordinate for the next box.
 278 Consider the top-left corner of the box $q(t(s)) = q(t)$
 279 and the bottom-right corner $r(f(s)) = r(f)$.

Because $p^x(s) = q^x(t)$,

$$t = \frac{p^x(s) - q_0^x}{v^x} = \frac{p^x - q_0^x + sv^x}{v^x} \quad (4)$$

Because our boxes are square,

$$r(f) = r_0 + fw = q_0 + tv + a \begin{bmatrix} 1 \\ -1 \end{bmatrix} \quad (5)$$

From (5),

$$f = \frac{1}{w^y}(q_0^y + tv^y - a - r_0^y) \quad (6)$$

$$a = r_0^x + fw^x - q_0^x - tv^x \quad (7)$$

Substituting equations (4) and (6) into equation (7) and
 solving for a ,

$$a(s) = \hat{\alpha}_o s + \hat{\beta}_o \quad (8)$$

where

$$\hat{\alpha}_o = \frac{u^x |w \times v|}{v^x (w^x + w^y)} \quad (9)$$

and

$$\hat{\beta}_o = \frac{|w \times v|(p_0^x - q_0^x) + v^x(|r_0 \times w| + |w \times q_0|)}{v^x (w^x + w^y)} \quad (10)$$

280 3.4.2. Finding $a(s)$ – adjacent case

Consider the top-left corner of the box $q(t(s)) = q(t)$
 and the bottom-left corner $r(f(s)) = r(f)$. $r(f)$ is now
 defined as

$$r(f) = r_0 + fw = q_0 + tv + a \begin{bmatrix} 0 \\ -1 \end{bmatrix} \quad (11)$$

Equations (4) and (6) remain the same while (7) be-
 comes

$$0 = r_0^x + fw^x - q_0^x - tv^x \quad (12)$$

Substituting equations (4) and (6) into equation (12) and
 solving for a ,

$$a(s) = \hat{\alpha}_a s + \hat{\beta}_a \quad (13)$$

where

$$\hat{\alpha}_a = \frac{u^x}{v^x w^x} \quad (14)$$

and

$$\hat{\beta}_a = \frac{w^x(p_0^x - q_0^x) + |w \times q_0| + |r_0 \times w|}{w^x} \quad (15)$$

281 3.4.3. Sampling

In both the *opposite* and the *adjacent* cases, $a(s)$ is of the form $a(s) = \hat{\alpha}s + \hat{\beta}$. We now use $a(s)$ to construct a sequence of values $S = \{s_0, s_1, s_2, \dots, s_n\}$ that meet our sampling criterion. We first construct the even samples (see figures 4b and 4e). Given a starting point $p(s_0)$,

$$p^x(s_{i+2}) = p^x(s_i) + a(s_i) \quad (16)$$

Substituting in equations (3) and (8)/(13),

$$p_0^x + s_{i+2}u^x = p_0^x + s_i + \hat{\alpha}s_i + \hat{\beta} \quad (17)$$

Solving for s_{i+2} gives the recurrence relation

$$s_{i+2} = \alpha s_i + \beta \quad (18)$$

where

$$\alpha = 1 + \frac{\hat{\alpha}}{u^x} \quad (19)$$

and

$$\beta = \frac{\hat{\beta}}{u^x} \quad (20)$$

Constructing the odd samples is identical, except that we start at

$$s_1 = \left(1 + \frac{\hat{\alpha}}{2u^x}\right)s_0 + \frac{\hat{\beta}}{2} \quad (21)$$

282 which is the point in the center of the first box in the
283 x -dimension.

We solve the recurrence relation (18) using the characteristic polynomial to yield

$$s_i = k_1 + k_2\alpha^i \quad (22)$$

where the k variables are split into those for even values of i and those for odd values of i , and are given as

$$k_1^{even} = \frac{\beta}{1 - \alpha} \quad (23)$$

$$k_1^{odd} = \frac{\beta}{1 - \alpha} \quad (24)$$

$$k_2^{even} = \frac{\alpha s_0 + \beta - s_0}{\alpha - 1} \quad (25)$$

$$k_2^{odd} = \frac{\alpha s_1 + \beta - s_1}{\alpha - 1} \quad (26)$$

The last step to formulating P for parallel computation is to determine how many samples we will need. Let $p(s_{exit})$ be the point at which the line p exits the cell.

$$k_1 + k_2\alpha^i < s_{exit} \quad (27)$$

results in

$$i < \log_{\alpha} \frac{s_{exit} - k_1}{k_2} \quad (28)$$

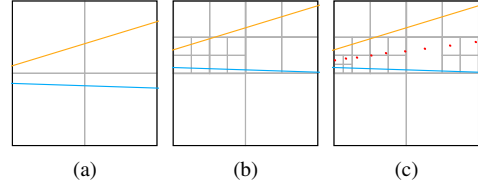


Figure 5: Best and worst cases given two lines. The same number of conflict resolution samples are generated regardless of where the lines are located. (a) Base case: two lines can be resolved by a single quadtree subdivision. (b) Worst case: the same two lines translated slightly in y now require five subdivisions to be resolved. (c) The number of cells generated from the shown resolution samples is within a constant factor of the worst case.

284 3.4.4. Iteration

285 Because conflict cell resolution only considers two
286 facets at a time, we may have to iterate multiple times
287 if more than two facets intersect a given cell. If new
288 sample points were found then we add them to the cur-
289 rent set S of sample points and return to building the
290 quadtree from points (section 3.1). We finish when the
291 only conflicts identified are at the maximum depth.

292 3.5. Optimality

293 Define an optimal final quadtree to be one in which
294 only conflict nodes have children, and let an optimal
295 final quadtree's size be n total nodes. Our iterative
296 sampling algorithm results in a quadtree that has a size
297 within a constant factor of n in the worst case (see figure
298 5). We omit the proof as well as an average case analysis
299 because optimality can be achieved by simply removing
300 unnecessary nodes in one final parallel pruning step.

301 4. Implementation

302 We have implemented¹ our algorithm using OpenCL.
303 Figure 6 shows the stages of the major kernels. Ev-
304 ery kernel call is parallel on vertices, facets, quadtree
305 nodes or Morton code bits. Our implementation uses
306 64-bit Morton codes, which were sufficient for all of
307 our datasets. There is no way of knowing *a priori*
308 what the object spacing is going to be, however, 64-bit
309 codes were sufficient for the most demanding datasets
310 while retaining reasonable radix-sort timings. Choos-
311 ing a large number of bits for the Morton code results
312 in little or no wasted effort in later refinement, affecting
313 the amount of later pruning only if intra-object vertex

¹Source code is available at www2.cose.isu.edu/~edwajohn/research/pquad.

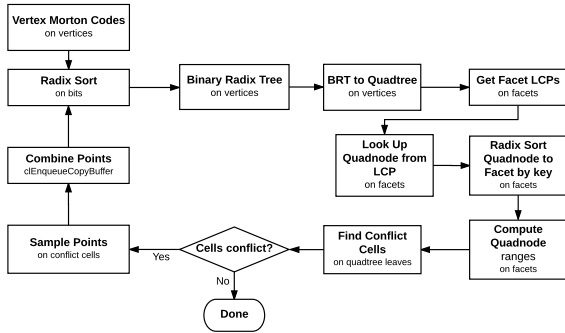


Figure 6: Kernel calls, with some calls omitted for clarity. The name of the kernel is in larger font while the the elements on which the parallelism runs are given in smaller font. The majority of calls are facet- or vertex-parallel.

314 spacing is small compared to spacing between objects.
 315 The number of bits also has no effect on the number of
 316 conflict cells unless the Morton codes are too small to
 317 resolve vertices.

318 Our implementation of the algorithm supports poly-
 319 gons and polylines which needn't be manifold or con-
 320 nected. Intersecting lines are not handled as a special
 321 case, i.e., the quadtree is simply resolved to its maxi-
 322 mum depth. Special handling can be implemented per
 323 application as needed, e.g., for collision detection appli-
 324 cations.

325 5. Results and conclusions

326 All tests were run on an Intel i7 6500u 3.10 GHz dual
 327 core processor, 8 GB of memory and an Nvidia GTX
 328 1070 graphics card. Figure 7 shows results a simple toy
 329 dataset showing conflict cell detection and resolution.
 330 A very complex dataset with many objects at very dif-
 331 ferent scales is shown in figure 8. It demonstrates that
 332 our method can handle datasets far beyond the mem-
 333 ory limits of uniform grid approaches while still fully
 334 resolving between objects. The gears dataset (figure
 335 9) again shows a large domain-to-object-spacing ratio,
 336 as well as non-convexities. The vascular dataset shown
 337 in figure 10 demonstrates our method on polylines de-
 338 rived from biological image data, which is often noisy
 339 with non-manifoldness and intersections. Table 1 shows
 340 timings for our implementation compared to the previ-
 341 ous state-of-the-art. Our implementation is significantly
 342 faster and also generates fewer quadtree cells. See Ap-
 343 pendix A for a runtime complexity analysis.

344 As can be seen in table 1, there is overhead with
 345 our approach: running our algorithm on small datasets
 346 yields smaller gains. In fact, our approach actually per-

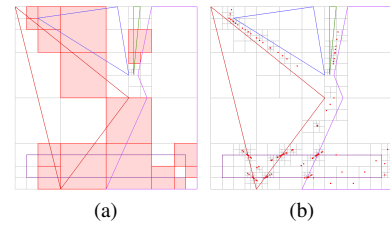


Figure 7: (a) A toy dataset showing conflict cells after building the quadtree from object vertices. (b) The toy dataset showing how samples are collected.

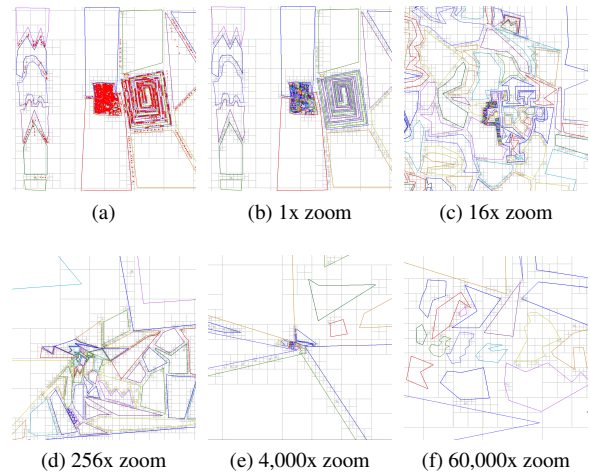


Figure 8: (a) A complex dataset with 470 objects at vastly different scales in object size and spacing. (b)-(f) Complex dataset at different zoom levels up to 60K magnification. This shows the importance of an adaptive method such as a quadtree. A uniform grid would require 2^{48} cells to resolve between objects. The quadtree shown here has 22,429 cells.

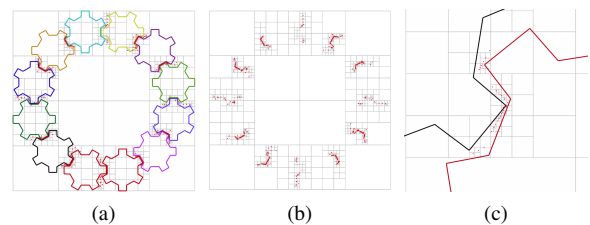


Figure 9: (a) A dataset of gears with close tolerance. The resolved quadtree with sampled points is shown. (b) Showing just the quadtree and sample points. (c) A zoomed-in image showing the close object spacing compared to the large domain.

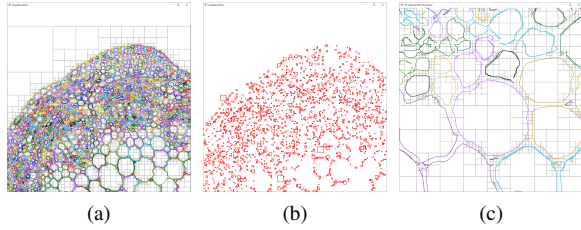


Figure 10: A large set of uniquely labeled polygons constructed from connected component analysis on a photograph of vascular cambium, a type of plant tissue. (a) Initial vertex quadtree after pruning. (b) All conflict cells of the initial quadtree. (c) After conflict cell resolution. No quadtree cell intersects more than one object. Our method works even though objects in this dataset are often non-manifold and have self-intersections.

dataset	objects	object facets	quadtree depth	time (millisec)	
				Ours	Prev
Fig. 7a	5	24	9	5	3
Fig. 9	12	288	10	8	24
Fig. 8a	470	4943	24	40	277
Fig. 10	2162	39,338	12	36	376

Table 1: Table of quadtree computation statistics and timings. *Ours* is the approach described in this paper and *Prev* is the approach by Edwards et al. [1]. Columns are: *objects* - the number of objects in the dataset; *object facets* - the number of line segments (2D) of all objects in the dataset; *quadtree depth* - required quadtree depth in order to resolve objects; *time (ms)* - milliseconds to build the quadtree

forms worse on the toy dataset. The power of our algorithm becomes obvious on large, complex datasets, where our performance time gains are significant.

Figure 11 shows the results of a scaling study, where we increased the number of objects and facets by orders of magnitude. Our algorithm consistently shows timings an order of magnitude faster than the state of the art. The approach of Edwards et al. failed on datasets with 10^6 facets or more.

As noted in the introduction, our continuing work is in fast construction of octrees modeling inter-object space in 3D. Every step in our method has a straightforward extension to 3D with the exception of point sampling for conflict resolution (see section 3.4), which is where we are focusing our efforts.

[1] Edwards J, Daniel E, Pascucci V, Bajaj C. Approximating the generalized voronoi diagram of closely spaced objects. *Computer Graphics Forum* 2015;34(2):299–309.
 [2] Karras T. Maximizing parallelism in the construction of BVHs, octrees, and k-d trees. In: *Proceedings of the Fourth ACM SIGGRAPH/Eurographics conference on High-Performance Graphics*. Eurographics Association; 2012, p. 33–7.
 [3] Lavender D, Bowyer A, Davenport J, Wallis A, Woodwark J. Voronoi diagrams of set-theoretic solid models. *Computer Graphics and Applications*, IEEE 1992;12(5):69–77.

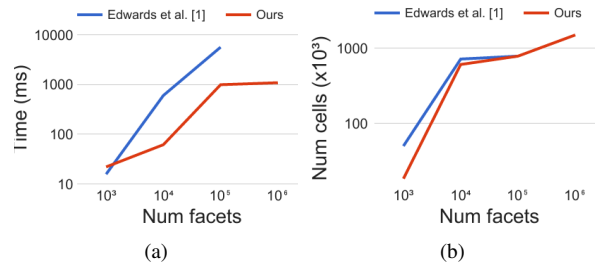


Figure 11: Scaling tests. The dataset used is a square domain with increasing numbers of non-intersecting lines. (a) Our algorithm consistently performs an order of magnitude faster than the algorithm of Edwards et al. [1] as the number of facets increases. (b) The quadtree that we build is roughly equal in size to that of the previous work.

[4] Strain J. Fast tree-based redistancing for level set computations. *Journal of Computational Physics* 1999;152(2):664–86.
 [5] Frisken SF, Perry RN, Rockwood AP, Jones TR. Adaptively sampled distance fields: a general representation of shape for computer graphics. In: *Proceedings of the 27th annual conference on Computer graphics and interactive techniques*. ACM Press/Addison-Wesley Publishing Co.; 2000, p. 249–54.
 [6] Boada I, Coll N, Sellares J. The voronoi-quadtree: construction and visualization. *Eurographics 2002 Short Presentation* 2002;;349–55.
 [7] Boada I, Coll N, Madern N, Antoni Sellares J. Approximations of 2D and 3D generalized Voronoi diagrams. *International Journal of Computer Mathematics* 2008;85(7):1003–22.
 [8] Teichmann M, Teller S. Polygonal approximation of Voronoi diagrams of a set of triangles in three dimensions. In: *Tech Rep 766, Lab of Comp. Sci., MIT*. 1997..
 [9] Vleugels J, Overmars M. Approximating Voronoi diagrams of convex sites in any dimension. *International Journal of Computational Geometry & Applications* 1998;8(02):201–21.
 [10] Bédorf J, Gaburov E, Portegies Zwart S. A sparse octree gravitational N-body code that runs entirely on the GPU processor. *Journal of Computational Physics* 2012;231(7):2825–39.
 [11] Zhou K, Gong M, Huang X, Guo B. Data-parallel octrees for surface reconstruction. *Visualization and Computer Graphics*, IEEE Transactions on 2011;17(5):669–81.
 [12] Li Z, Wang T, Deng Y. Fully parallel kd-tree construction for real-time ray tracing. In: *Proceedings of the 18th meeting of the ACM SIGGRAPH Symposium on Interactive 3D Graphics and Games*. ACM; 2014, p. 159–.
 [13] Baert J, Lagae A, Dutré P. Out-of-core construction of sparse voxel octrees. In: *Proceedings of the 5th High-Performance Graphics Conference*. ACM; 2013, p. 27–32.
 [14] Crassin C, Neyret F, Lefebvre S, Eisemann E. Gigavoxels: Ray-guided streaming for efficient and detailed voxel rendering. In: *Proceedings of the 2009 symposium on Interactive 3D graphics and games*. ACM; 2009, p. 15–22.
 [15] Laine S, Karras T. Efficient sparse voxel octrees. *Visualization and Computer Graphics*, IEEE Transactions on 2011;17(8):1048–59.
 [16] Lefebvre S, Hoppe H. Compressed random-access trees for spatially coherent data. In: *Proceedings of the 18th Eurographics conference on Rendering Techniques*. Eurographics Association; 2007, p. 339–49.
 [17] Choi B, Komuravelli R, Lu V, Sung H, Bocchino RL, Adve SV, et al. Parallel SAH kd tree construction. In: *Proceedings of*

417 the Conference on High Performance Graphics. Eurographics
418 Association; 2010, p. 77–86.

419 [18] Bastos T, Celes W. GPU-accelerated adaptively sampled distance
420 fields. In: Shape Modeling and Applications, 2008. SMI
421 2008. IEEE International Conference on. IEEE; 2008, p. 171–8.

422 [19] Park T, Lee SH, Kim JH, Kim CH. CUDA-based signed distance
423 field calculation for adaptive grids. In: Computer and
424 Information Technology (CIT), 2010 IEEE 10th International
425 Conference on. IEEE; 2010, p. 1202–6.

426 [20] Yin K, Liu Y, Wu E. Fast computing adaptively sampled distance
427 field on GPU. In: Pacific Graphics Short Papers. The Eurographics
428 Association; 2011, p. 25–30.

429 [21] Crassin C, Green S. Octree-based sparse voxelization using the
430 GPU hardware rasterizer. OpenGL Insights 2012::303–18.

431 [22] Kim YJ, Liu F. Exact and adaptive signed distance fields computation
432 for rigid and deformable models on GPUs. IEEE Transactions on
433 Visualization and Computer Graphics 2014;20(5):714–
434 25.

435 [23] Ha L, Krüger J, Silva CT. Fast four-way parallel radix sorting
436 on GPUs. In: Computer Graphics Forum; vol. 28. Wiley Online
437 Library; 2009, p. 2368–78.

438 [24] Pantaleoni J. VoxelPipe: a programmable pipeline for 3D voxel-
439 ization. In: Proceedings of the ACM SIGGRAPH Symposium
440 on High Performance Graphics. ACM; 2011, p. 99–106.

441 Appendix A. Complexity analysis

442 Let $M = |F|$ and $N = |V|$, where F are the object
443 facets and V are the object vertices. Let D be the depth
444 of the quadtree, and D_{max} be the maximum depth of the
445 quadtree. In this analysis we assume sufficient parallel
446 units to maximize parallelization.

447 Time complexity

- 448 1. Build quadtree using Karras’ algorithm [2], including
449 pruning - $O(D_{max})$.
- 450 2. Detect conflict cells
 - 451 (a) Build BCells array - $O(D)$. Building of the array
452 runs in parallel for each facet f . The facet
453 looks at each vertex (we assume simplices
454 with a constant number of dimensions), computes
455 Morton codes and finds the longest
456 common prefix among vertices. This requires
457 looking at each bit, of which there are $O(D)$.
 - 458 (b) Sort BCells array - $O(D_{max})$. We use a parallel
459 radix sort with linear complexity dependent
460 on the max quadtree depth.
 - 461 (c) Index BCells with quadtree data structure
462 - $O(D)$. This runs in parallel on leaf cell
463 IDs and each kernel requires a search of the
464 quadtree for a given cell ID, taking at most D
465 steps.
 - 466 (d) Find facets that intersect each leaf cell -
467 Worst case $O(M + D)$, average case $O(D)$. In

468 unusual datasets, a single leaf cell will be in-
469 tersected by $O(M)$ facets. On average, how-
470 ever, leaf cells intersect a small number of
471 facets, and thus this step is dominated by the
472 depth D of the quadtree due to visiting each
473 ancestor of the leaf cell.

474 3. Resolve conflict cells

- 475 (a) Compute new sample points - $O(1)$. The first
476 step computes, in parallel over conflict cells,
477 the number of samples required to resolve the
478 cell using equation (28). The second step is
479 to compute the samples themselves, which is
480 done in parallel over all new samples to be
481 computed, using equation (22).

- 482 (b) $S \leftarrow S \cup S' - O(1)$.

- 483 4. Iterate - $O(Q)$ iterations. In the worst case, all
484 facets intersect a single cell, requiring potentially
485 $Q = O(M^2)$ iterations. In our testing, Q has not
486 exceeded 4.

487 The final complexity of each iteration is $O(M + D_{max})$
488 worst case and $O(\log M + D_{max})$ average case. In prac-
489 tice we must fix the depth of the quadtree to a constant
490 value in order to use a predetermined integer size for the
491 Morton codes, which brings the average case complex-
492 ity to $O(\log M)$. Taking iteration into account, the final
493 complexity is $(Q \log M)$ average case.

494 Space complexity

495 The primary data structures are shown in figure 3a.
496 The quadtree data structure is size $O(|S|)$ and the re-
497 maining arrays are of size M . As $|S| \geq M$, our final
498 space complexity is $O(|S|)$. The number of samples in
499 S depends on the dataset. In 2D, in the worst case, the
500 facets can form an arrangement of maximum number of
501 intersections, which is $M(M - 1)/2 = O(M^2)$. If this
502 is the case then we subdivide to the maximum quadtree
503 depth at each intersection, causing a quadtree of size
504 $O(DM^2)$.